metals

MDPI

Article

Erosion-Corrosion of Gathering Pipeline Steel in Oil-Water-Sand Multiphase Flow

Qiang Li * and Bingcheng Liu

Institute of Climate Change and Energy Sustainable Development, Qingdao University of Science and Technology, Qingdao 266061, China

* Correspondence: qiangli@qust.edu.cn; Tel.: +86-532-8895-9577

Abstract: This work studies a series of factors influencing erosion-corrosion in oilfield gathering pipelines steel using the home-made testing pipe flow loop. Results showed that steel was corroded in oil-water flow. The corrosion rate increased with the flow velocity on the whole, and the addition of solid particles would intensify the localized corrosion. For the erosion-corrosion test added with 2 wt% quartz sand at the velocity of 2 m/s, the portion of pure corrosion and pure erosion accounted for 47.50% and 70.83%, respectively. The erosion-enhanced corrosion was 16.67% of the total weight loss, while the corrosion inhibiting the damage from erosion accounted for 35.00%, so negative synergistic effects appeared in the oil-water-sand multiphase flow conditions.

Keywords: pipelines; erosion; corrosion; EIS

1. Introduction

Erosion-corrosion is common in oil and gas production plants and pipelines where there is an interaction between solid particles, corrosive fluid and target materials [1–3]. Previous studies [4,5] have shown that the components of erosion and corrosion are not mutually exclusive and instead interact to exacerbate the damage to a greater extent than the sum of the separate parts. Synergism of erosion and corrosion can result in more significant material loss than that caused individually [4,6,7]. Several investigations [8–10] have been reported to study the erosion-corrosion phenomena involved.

The failure of a subsea crude oil pipeline, which led to oil leakage, has been reported to occur after 27 years of service. The investigation results suggest that the cause of failure is electrochemical corrosion combined with the mechanical process, known as flow-induced corrosion [11]. Gathering pipelines in oilfields are seriously damaged by erosion-corrosion, which results from media including oil, gas, water and sand grains in the brine [12], so it is multiphase flow erosion-corrosion [13,14]. Because of the various compositions of oilfield brines, the mechanism of multiphase flow corrosion-erosion on the inner wall of gathering pipelines is very complex and not clear [15,16]. It is of great significance for safe field production to work out effective countermeasures by studying the mechanism based on oilfield conditions.

Despite various studies performed to study erosion-corrosion in the two-phase flow, including gas-sand and/or sand-water medium, there has been very limited study focusing on the erosion-corrosion in oil-water-sand conditions [17], which is the common case in oilfields. Stack et al. [18] studied the erosion-corrosion performance of carbon steel in oil-water solutions with varying portions of petroleum and water through a jet impingement test rig. They stated that the extent of erosion changed with the portion of oil. Tang et al. [5] studied the erosion-corrosion mechanism of X65 pipe steel in a simulated oil-sand slurry through an impingement jet system. They suggested that erosion dominated the erosion-corrosion of X65 steel in the oil-sand slurry because erosive particles would continually destroy the passivity of the steel developed in the oil-water emulsion. Wongpanya et al. [16] studied the erosion-corrosion behavior of 1045 and J55 steels in crude oil (16% water in

check for updates

Citation: Li, Q.; Liu, B. Erosion-Corrosion of Gathering Pipeline Steel in Oil-Water-Sand Multiphase Flow. *Metals* **2023**, *13*, 80. https://doi.org/10.3390/met13010080

Academic Editor: Liang Zhou

Received: 4 November 2022
Revised: 16 December 2022
Accepted: 21 December 2022
Published: 28 December 2022

volume percentage) with sand using an impingement jet system. They found that the major cause of the wastage of low-alloy steel was the erosion process. Meng et al. [19] studied the corrosive wear property of oil tubing in sand-oil-water (crude oil and formation water) using a rotating disc-type corrosive wear tester and suggested that a heavier worn loss of the samples in sand-oil-water (oilfield brine) than that in sand-water (clean water) liquid. Peng et al. [17] studied the erosion of pipe bend and plugged tee by solid particles in oil-water-sand multiphase flow with CFD simulation. They analysed the relationship between solid particles and pipe erosion and predicted the maximum erosion position in the pipe bend and plugged tee. Obviously, the presence of oil will affect the erosion-corrosion behavior of steels in the multiphase flow, both the pure corrosion rate and the total erosion-corrosion rate decrease when there is a large portion of oil in the flow. This is because oil can wet the pipeline surface and serve as a physical barrier to isolate the steel from the corrosive environment. However, the chance of oil-wetting could be very low, or there will be very limited pipeline surface that can be wetted by oil [20] when the portion of oil in the multiphase flow is small. Considering the complexities brought in by oil, more research on the erosion-corrosion behavior of pipeline steel in oil-water-sand multiphase flow is thus required.

Of all the erosion-corrosion tests performed in the oil-water-sand flow, jet impingement testers were the most widely used. This is because jet impingement testers have the advantage [21] of being easy to control the impingement velocity and the impact angle. However, the flow regime in the jet impingement could be different from the actual conditions. In contrast, a pipe flow loop, which has a similar structure to the actual pipelines, is a more appropriate device for erosion-corrosion testing. By ingenious design, erosion-corrosion at different locations of a pipeline section can also be measured [22]. Thus, it is more advisable to use a pipe flow loop in multiphase flow erosion-corrosion tests.

With the study object material of 20$^{\#}$ steel that is commonly used in oilfield gathering pipelines for its good mechanical properties and low cost [23,24], a series of tests were done on the home-made erosion-corrosion pipe flow loop using the weight-loss method, polarization curve and Electrochemical Impedance Spectroscopy (EIS). Erosion-corrosion behavior of 20$^{\#}$ steel in the oil-water-sand flow under various conditions was studied, and the erosion-corrosion mechanism was discussed.

2. Materials and Methods

2.1. Materials and Solution

The 20$^{\#}$ steel was selected as the testing material, and it was composed of (wt%) C 0.200, Si 0.210, Mn 0.410, P 0.015, S 0.007, Cr 0.060, Cu 0.160, Ni 0.050 and Fe balance. The oilfield brine that was directly retracted from Guangli Gathering Station in Shengli Oilfield was used as the fluid phase of the testing medium. It consisted of trace amount of oil (around 100 ppm), and the concentration of ionic compositions is presented in Table 1. Besides, this test was done in a semi-open system at room temperature with dissolved oxygen of 7.25 mg/L, free CO_2 of 25.3 mg/L, pH 7.57, and conductivity of 37.5 ms/cm.

Table 1. Chemical composition of oilfield brine.

Constituents	Concentration (mg/L)
Na^++K^+	14,887
Ca^{2+}	1523
Mg^{2+}	369
NH_4^+	115
Cl^-	25,098
SO_4^{2-}	2257
HCO_3^-	308
NO_3^-	105

Solid particles are commercially available quartz sand (Laiwushi Luzhong Shiyingfen Co., Ltd., Laiwu, China) that was purified, washed repeatedly, and dried before screening. The size of quartz sand particles used in the tests was between 300 μm and 450 μm.

2.2. Pipe Flow Loop Setup

The home-made pipe flow loop is shown in Figure 1. This setup comprises several functional systems, including a slurry feed system (includes the slurry tank and the stirrer), a pipe flow circulation regulating system (includes the slurry pump, the two stop valves and the electromagnetic flowmeter), an erosion-corrosion testing system (i.e., the pipe flow testing section, the three-electrode system and the electrochemical working station), and a temperature controlling system (includes the cryostat circulator and the connected heat exchange tubes, and the thermocouple). These systems can regulate velocity (maximum 3 m/s), sand concentrations (maximum 10 wt% with a particle diameter no larger than 1 mm) and electrode positions, and meet the requirements of weight loss testing and online electrochemical testing.

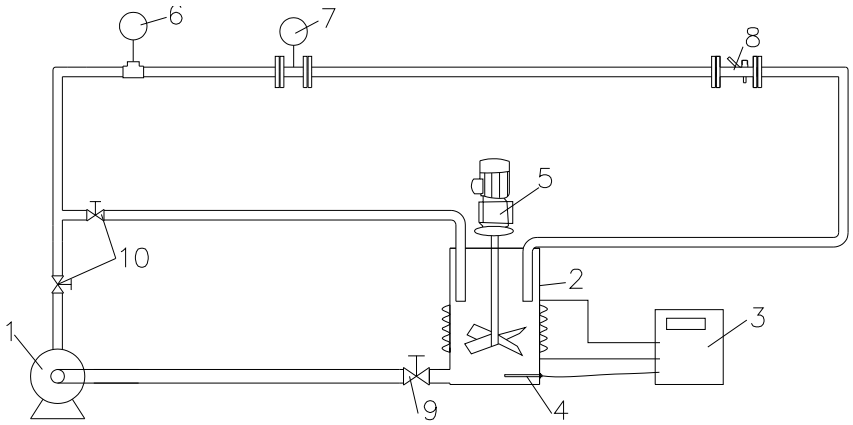

Figure 1. Schematic diagram of the erosion-corrosion testing rig (1—slurry pump, 2—slurry tank, 3—cryostat circulator, 4—thermocouple, 5—stirrer, 6—pressure gage, 7—electromagnetic flowmeter, 8—pipe flow testing section, 9—ball valve, 10—stop valve).

The testing section, which has an inner diameter of 25 mm and a length of 150 mm, is shown in Figure 2a. Its main body is an acrylic tube with flanges on two ends and three branch pipes installed on the tube for the working electrode, reference electrode, and counter electrode. The three pipes are in a position similar to that of the three-electrode system, in which the three pipes share the same plane and the working electrode pipe and counter electrode pipe share the same axis. The reference electrode pipe is set to have a 45° angle relative to the working electrode pipe to reduce the distance between the reference electrode and the working electrode. Twelve holes are set on the flanges to ensure a ±90° regulation of angles on a horizontal level at an interval of 30°. The working electrode (Figure 2b) fits the testing section, and the working surface has the same cambered surface with the curvature of the inner wall of the tube. Before the test, except for the working surface, the sample was coated with Vaseline and Teflon thread seal tape to ensure that only the working surface was exposed to the solution.

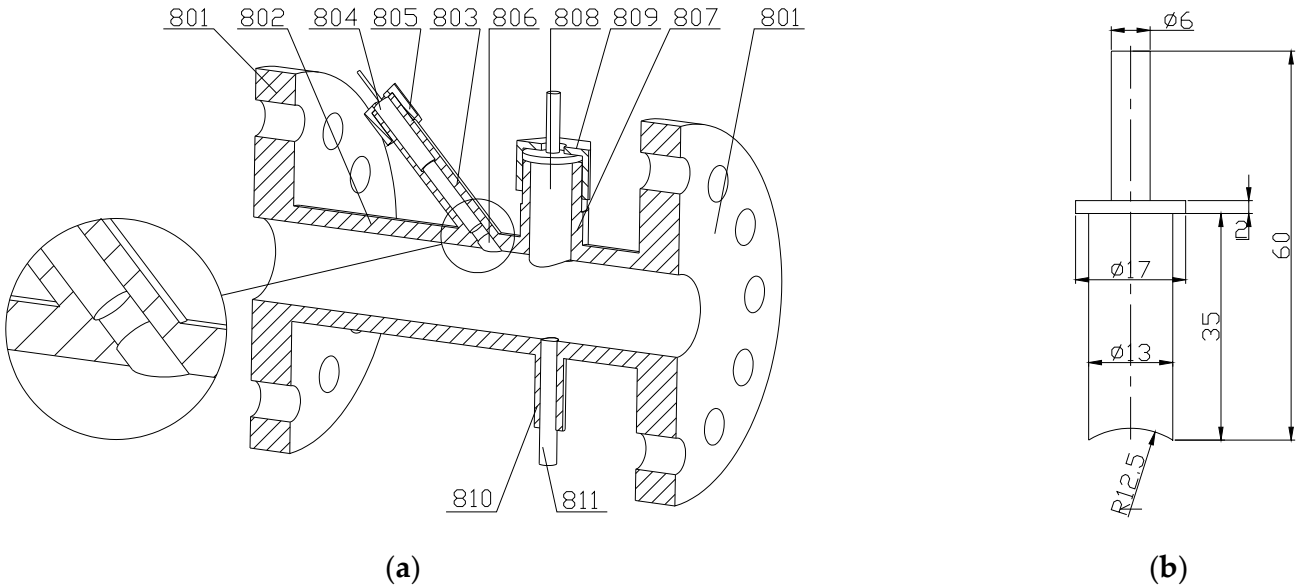

Figure 2. Schematic diagram of ((**a**): 801—flange, 802—acrylic tube, 803—reference electrode installing pipe, 804—reference electrode, 805—nut of the reference electrode, 806—porous material, 807—working electrode installing pipe, 808—working electrode, 809—nut of the working electrode, 810—auxiliary electrode installing pipe, 811—auxiliary electrode) the pipe-flow testing section and (**b**) the working electrode (mm).

2.3. Testing Methods

The electrode's working surface, which had a surface area of 1.403 cm^2, was polished from 220$^{\#}$ to 1000$^{\#}$ using the waterproof abrasive paper, and then it was washed with distilled water and wiped with acetone before being dried and put in a drying basin for later use.

Electrochemical testing was carried out on a CHI660D electrochemical station (Shanghai CH Instruments Co. Ltd., Shanghai, China) with a Ag/AgCl reference electrode (saturated KCl, Shanghai CH Instruments Co., Ltd., Shanghai, China) and a carbon rod auxiliary electrode (Shanghai Yueci Electronic Technology Co., Ltd., Shanghai, China). The scanning rate of the polarization curve was 0.5 mV/s, and the scanning section was ±250 mV relative to open circuit potential. The amplitude of EIS was 10 mV with the scanning range of 100,000~0.05 Hz.

This work focused on the erosion-corrosion problem in straight gathering liquid pipes. Flow velocities and sand concentrations were selected accordingly. For a straight pipe, an economical velocity of 1 m/s was suggested [25]. However, a relatively large flow velocity of 2 m/s was also seen in the field [26]. As a result, the flow velocity was controlled to be no larger than 2 m/s. For the oilfield brine without sand, EIS tests were performed for five flow velocities: 0, 0.5, 1, 1.5 and 2 m/s. Sand concentrations in the flow vary with different oil reservoirs, a sand concentration range of 0.5~2 wt% was selected by referring to the literature [27]. Noting that under-deposit corrosion could happen for a sandy fluid with a zero-flow velocity, thus this condition was not considered to avoid making the corrosion system more complex. So, for the oilfield brine with sand, EIS tests were performed for flow velocities of 0.5, 1, 1.5 and 2 m/s while the sand concentration was 2 wt%, and for sand concentrations of 0.5, 1, 1.5 and 2 wt% while the flow velocity was 2 m/s. All electrochemical tests were performed after the experiment was run for a period of four hours.

A FA2004 precise balance (Shanghai Sunny Hengping Scientific Instrument Co., Ltd., Shanghai, China) at an accuracy of 0.1 mg was used in the weight-loss testing. For weight loss testing, the cleaned working electrode should be dried in a drying oven at 60 °C for 30 min and put in a dryer for at least 12 h before being weighed. Before weighing, the

same treatment was done to a parallel sample to rectify the weight loss from corrosion by chemical cleaning with the hydrochloric acid (Sinopharm Chemical Reagent Co., Ltd, Shanghai, China) and hexamethylene tetramine (Sinopharm Chemical Reagent Co., Ltd, Shanghai, China) solution [28]. Weight loss of the working electrode can be converted to corrosion current according to Faraday's law as follows:

$$iSt = \frac{\Delta m}{M} ZF \quad (1)$$

where i is the corrosion current density, A/cm^2; S is the working electrode surface area, cm^2; t is the exposure time, s; Δm is the weight loss, g; M is the molar weight of Fe, 55.85 g/mol; Z is the number of charges joining in the anodic process, 2; F is the Faraday's constant, 96,485 C/mol.

A Hitachi SU-1500S Scanning Electron Microscope (SEM) (Hitachi High Technologies Inc., Schaumburg, IL, USA) was used to examine the surfaces of working electrodes used in the erosion-corrosion tests. Secondary electron (SE) mode was applied, and the accelerating voltage was 15.0 kV. ImageJ software developed by the National Institutes of Health (NIH) was used to quantitatively evaluate the pit area on the steel surface [29].

3. Results and Discussion

3.1. Influence of Velocity on Erosion-Corrosion Performance

Results of EIS test in oilfield brine without sand and with 2 wt% sand under different velocities are shown in Figure 3. It shows that the size of the semi-circular plots generally tends to reduce as the flow velocity decreases, the flow velocity of 1.5 m/s seems to be an exception. For the same flow velocity, the EIS diagram obtained in the oilfield brine without sand was associated with a mono-capacitive loop, while double-capacitive loops appeared in the oilfield brine with 2 wt% sand. The capacitive loop that appeared at the low-frequency range could be due to the presence of pits resulting from the bumping or cutting action on the electrode surface arising from solid particles in the solution and/or corrosion pitting on the surface caused by the high concentration of Cl^-.

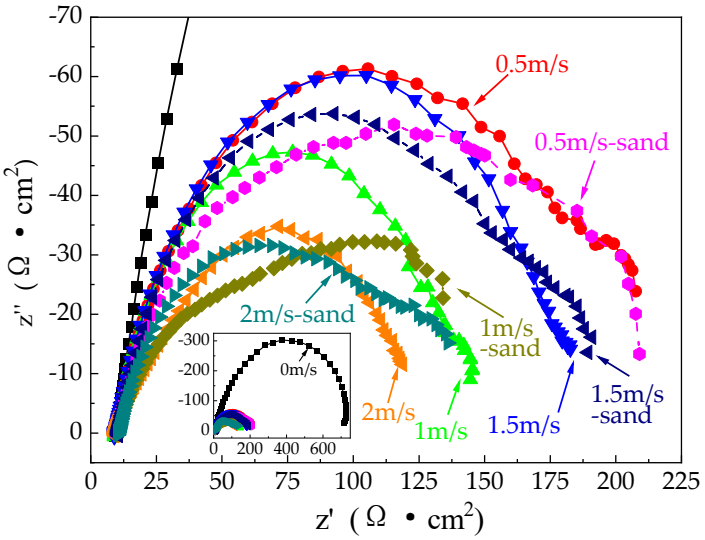

Figure 3. EIS diagram measured on 20$^{\#}$ steel in the oilfield brine with/without sand under different flow velocities.

The equivalent circuit diagrams shown in Figure 4 were used to fit the EIS plots shown in Figure 3, after which a quantitative analysis of the corrosion process could be performed. Specifically, Figure 4a was used to perform the fitting for the oilfield brine without sand. In this figure, R_s is the solution resistance between the boundary of the reference electrode and that of the working electrode, *CPE* is the equivalence element of the double electrode

layer between the electrode interface and solution, and R_p is the polarization resistance. Figure 4b, which includes an additional pair of constant phase element and resistance that represent the corrosion process in the pits, was used for the fitting in the oilfield brine with 2 wt% sand. In this figure, CPE_1 is the equivalence element of the double electrode layer between electrode and solution, R_{p1} is the polarization resistance of the whole electrode, CPE_2 is the equivalence element of the double electrode layer inside corrosion pits, and Rp_2 is the polarization resistance of electrode corroded inside the pits.

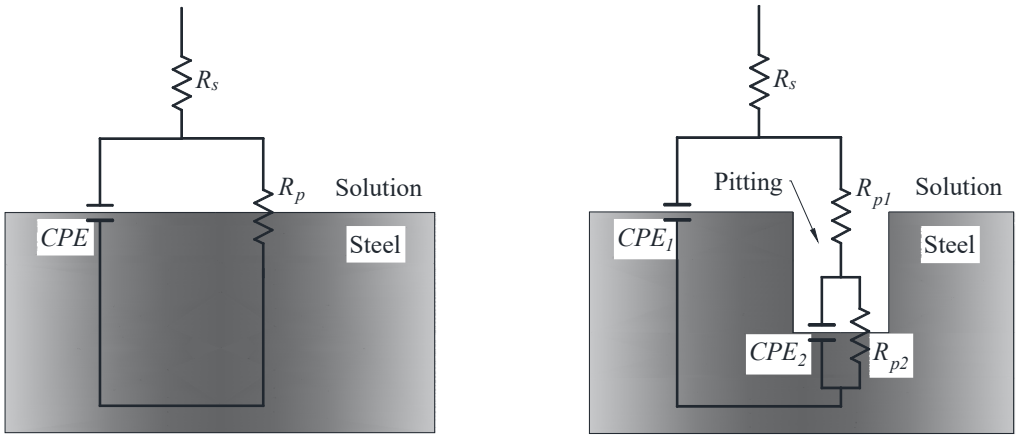

(**a**) (**b**)

Figure 4. Electrochemical equivalent circuit for the corrosion system: (**a**) without sand, (**b**) with 2 wt% sand.

Values of R_p were obtained after fitting Figure 3. The curves shown in Figure 5a were plotted with different velocities as the abscissa axis and values of R_p as the vertical axis. It shows that when the fluid velocity increased from 0 to 0.5 m/s, the R_p was associated with a profound decrease. When the flow velocity continually increased from 0.5 m/s to 2 m/s, the R_p decreased overall but at a smaller rate. The value of R_p has an inverse relation to the corrosion rate: a higher R_p is associated with a low corrosion rate. Thus, it can be determined from Figure 5a that with the growth of velocity, the corrosion rate was in a tendency of going up on the whole, but the increase rate became smaller as the velocity increased.

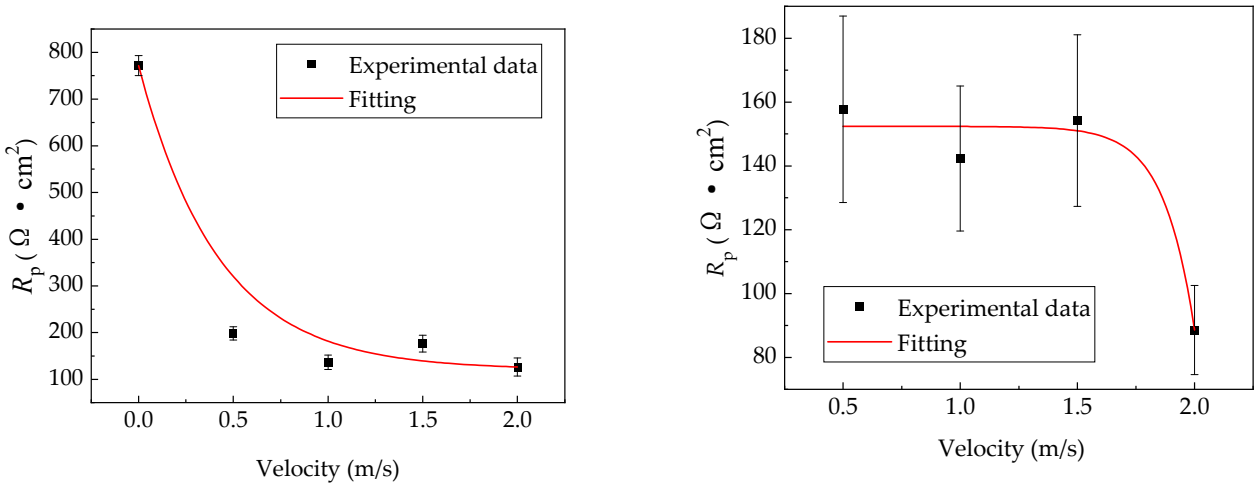

(**a**) (**b**)

Figure 5. Diagram of a relationship between velocity and R_p in oil-water flow: (**a**) without sand, (**b**) 2 wt% sand.

Reactions on the cathodic electrode, such as oxygen adsorption corrosion and HCO_3^- corrosion, may occur because of the dissolved oxygen and HCO_3^- in the solution. Cathodic reactions thus include:

$$O_2 + 2H_2O + 4e \rightarrow 4OH^- \quad (2)$$

$$2HCO_3^- + 2e \rightarrow H_2 + 2CO_3^{2-} \quad (3)$$

The anodic reaction involves the oxidation of iron to form ferrous ions:

$$Fe - 2e \rightarrow Fe^{2+} \quad (4)$$

Faster flow velocity can speed up the corrosion rate on 20# steel by compressing the thickness of the surface boundary layer and prompting mass transfer of cathodic reactive species, including oxygen and HCO_3^-, from the bulk solution to the steel surface. At the same time, a faster corrosion rate is accompanied by the formation of corrosion product film, i.e., $Fe(OH)_2$, $Fe(OH)_3$ and $FeCO_3$ (as shown in Equations (5)–(8)), on the steel surface to slow down the corrosion rate on the 20# steel. Corrosion product films are formed by [30–32]:

$$2OH^- + Fe^{2+} \rightarrow Fe(OH)_2 \quad (5)$$

$$4Fe(OH)_2 + O_2 + 2H_2O \rightarrow 4Fe(OH)_3 \quad (6)$$

$$2HCO_3^- + Fe^{2+} \rightarrow FeCO_3 + H_2O + CO_2 \quad (7)$$

$$CO_3^{2-} + Fe^{2+} \rightarrow FeCO_3 \quad (8)$$

Thus, both flow velocity and the formation of corrosion product film influence the corrosion rate.

Only average data on the electrode surface can be obtained from the EIS test in the corrosion of oil-water flow with sand, so the localized electrochemical information cannot be differentiated. Therefore, in this work, the relationship between velocity and overall corrosion (R_{p1}) was considered, which is displayed in Figure 5b. This figure shows that the corrosion rate went up slowly at first and then raised rapidly after the velocity reached a certain point, i.e., 1.5 m/s. This phenomenon is a result of the formation of corrosion product film and sand particles hitting the electrode surface and destroying the film. Under a slow velocity, the damage is so tiny that corrosion product film can still protect the electrode surface; when the velocity grows up to a certain level, the stronger and more frequent hitting on the surface undermines the protection of the corrosion product film, so the corrosion rate speeds up noticeably.

A comparison of Figure 5a,b shows that although the R_p was smaller in the oil-water-sand flow (indicating a larger corrosion rate) than that in the oil-water flow on the whole, there was no significant difference in R_p values between the two conditions. Because the variable R_p can only reflect the kinetics of the electrochemical process or the electrochemical corrosion rate, this result shows that the electrochemical corrosion process was not greatly enhanced by the sand, probably because the sand cannot always destroy the corrosion product film.

3.2. Influence of Sand Concentrations on Erosion-Corrosion

Figure 6 displays the EIS diagram measured on 20# steel in oil-water flow under different sand concentrations—0.5%, 1.0%, 1.5% and 2.0% at room temperature and a velocity of 2 m/s.

It can be seen from Figure 6 that a mono capacitive loop appeared on the diagram when the mass fraction of sand was lower than 2%, which indicates that a lower concentration of sand cannot speed up corrosive pitting. Thus, Figure 4a was used to fit the EIS diagram measured on 2# steel in oil-water flow with smaller sand concentrations while Figure 4b was used to fit the EIS diagram on 2# steel in oil-water flow with 2 wt% sand. Fitting results, as shown in Figure 7, show that with the increasing concentration of sand, polarization resistance went up before going down, while the corrosion rate went down before going

up. This result is due to the smaller scouring action of the sand on the electrode surface, and this action of sand can help remove the corrosion product on the surface to speed up the formation of passive film. Thus, the corrosion rate can be slowed down; with the concentration going higher, starting at a concentration of 1 wt%, the more frequent scouring action of sand will destroy the corrosion product and passive film, so the corrosion is accelerated [33].

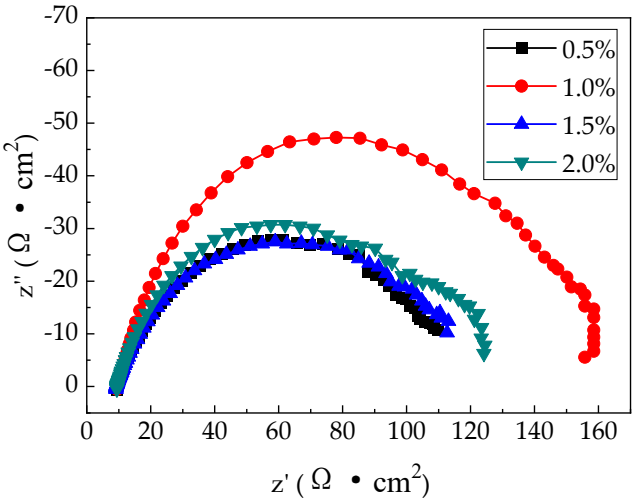

Figure 6. EIS diagram measured on 20# steel in oil-water flow under different sand concentrations.

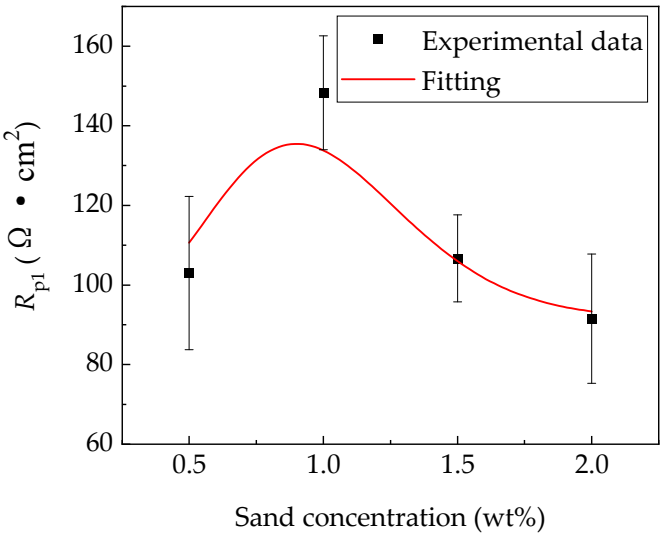

Figure 7. Diagram of the relationship between sand concentration and R_{p1} in oil-water flow.

3.3. Performance of Erosion-Corrosion at Different Angle Positions of a Pipe Section

EIS test results at different angle positions of a pipe section are shown in Figure 8. This figure shows that double capacitive loops appeared at all angle positions and all capacitive loops are basically the same, with minor differences in size. Thus, the corrosion mechanism at different positions is basically identical. Moreover, taking the unavoidable testing errors into consideration, corrosion behavior at different positions of a pipe section is nearly the same. While it was believed that the non-uniform distribution of flow velocity and particle concentration [22] in a tube is responsible for the different erosion-corrosion behavior at different locations, it could be concluded that there was only a minor difference in the flow velocity and particle concentration in the pipe flow.

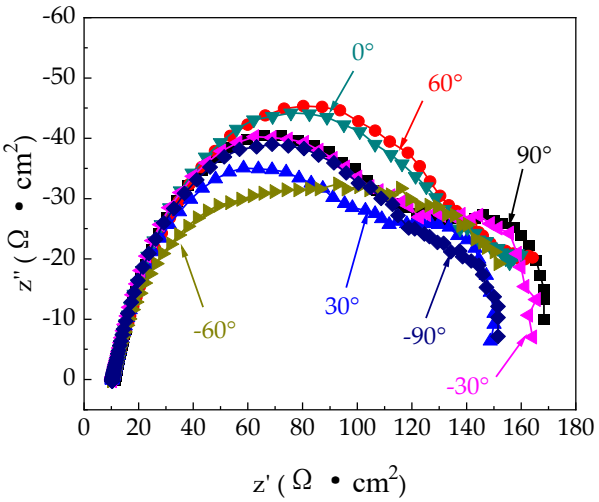

Figure 8. EIS diagram measured on 20# steel in oil-water-sand flow at different angle positions.

3.4. Erosion-Corrosion Synergism

A calculation of the portions of pure erosion, pure corrosion, corrosion-enhanced erosion and erosion-enhanced corrosion is needed, which is crucial to elucidate the mechanism of erosion-corrosion in this system. Pure corrosion means that the working electrode was put in the oilfield brine and scoured for 10 h at room temperature and the velocity of 2 m/s. The working electrode was scoured for 10 h with the addition of 2 wt% quartz sand and −950 mV (vs. Ag/AgCl) protective potential was exerted on the electrode to inhibit the corrosion in the pure erosion test. Before and after each test, the weight of the electrode was recorded multiple times before taking the average, with which weight loss data in each test condition was calculated.

Acceleration of erosion for corrosion can be calculated through Equation (9) [5]:

$$\Delta i_C = \frac{B_{oil-water-sand}}{R_{poil-water-sand}} - \frac{B_{oil-water}}{R_{poil-water}} \quad (9)$$

where $R_{poil\text{-}water}$ is the polarization resistance of 20# steel in the oil-water system and $R_{poil\text{-}water\text{-}sand}$ is the polarization resistance of 20# steel in the oil-water-sand system, both were obtained after the fitting of EIS. $B_{oil\text{-}water}$ and $B_{oil\text{-}water\text{-}sand}$ are the Stern-Geary coefficients of 20# steel in the oil-water system and the oil-water-sand system, respectively. Tafel curves of working electrodes, as shown in Figure 9, were measured in the oil-water system and the oil-water-sand system at the velocity of 2 m/s to obtain the two Stern-Geary coefficients. Fittings of β_a and β_c were done and substituted in Equation (10) to work out the value of B, as follows:

$$B = \frac{\beta_a \beta_c}{2.303(\beta_a + \beta_c)} \quad (10)$$

The corrosion-enhanced erosion-ΔE can be calculated through Equation (11) [34].

$$T = E + \Delta E + C + \Delta C \quad (11)$$

In Equation (11), T is the total weight loss in erosion-corrosion, E is the weight loss in pure erosion, and C is the weight loss in pure corrosion; ΔE is the weight loss due to corrosion-enhanced erosion, while ΔC is the weight loss arising from erosion-enhanced corrosion. The total weight loss and portions of pure corrosion, pure erosion and synergism are shown in Table 2.

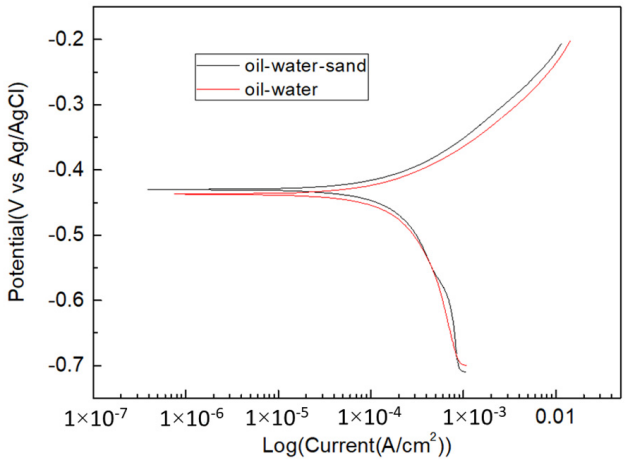

Figure 9. Tafel diagram measured in oil-water and oil-water-sand flow.

Table 2. Weight loss and portion of the pure corrosion, pure erosion and synergism.

-	*C*	*E*	Δ*C*	Δ*E*	*T*
Weight loss (mg)	5.7	8.5	2.0	−4.2	12.0
Portion	47.50%	70.83%	16.67%	−35.00%	100%

Table 2 reveals that pure erosion emerged as the dominating portion, followed by pure corrosion. Erosion could slightly accelerate corrosion, and the negative synergistic effect appearing in the whole system indicates that corrosion inhibits erosion.

Wood [35] summarized many processes that could lead to positive and negative interactive effects between mechanical and electrochemical processes under erosion-corrosion conditions. According to the analysis of negative interaction, the most likely cause for corrosion inhibiting erosion is that the corrosion product layer formed on steel surfaces could decrease friction between impacting solid particles and the bulk substrate material.

Corrosion product film itself can also reduce the contact of sand particles with the metal, and the compact $FeCO_3$ film formed in this system has stronger resistance to mechanical erosion, thus reducing the damage of erosion on the $20^{\#}$ steel to some extent.

3.5. Observation of Corrosion Morphology

Surface morphology pictures of the pure corrosion test electrode and the erosion-corrosion test electrode are displayed in Figures 10 and 11, respectively. Since the surface morphology at different areas of the working electrode varied, the morphology at the typical area is displayed in the figure. Comparing the morphology before chemical cleaning reveals that the corrosion product distributed unevenly on the electrode surface in two tests: sometimes was concentrated while sometimes was few and scattered. The product in the pure corrosion test was few and scattered, so its protection was quite poor, while the product in the erosion-corrosion test was quite compact, the film can effectively reduce the damage of erosion-corrosion on the electrode.

After the corrosion product was removed through chemical cleaning, the electrode surface was observed through an SEM again, and the morphology after cleaning in two tests is shown in Figures 10 and 11. A comparison of the two figures indicates that corrosion pits were formed on the surface in two tests: the number of corrosion pits was larger in the pure corrosion test, while the number of pits was smaller in the erosion-corrosion test. This is further illustrated by the ratio of pit area to the whole area obtained with ImageJ, as shown in Figure 12. The ratio of pit area to the whole area for the pure corrosion test electrode was determined to be 10.33%, while it was 8.43% for the erosion-corrosion electrode. At the same time, the corrosion pits on the pure electrode were more evenly distributed, compared with that of the erosion-corrosion electrode. Thus, adding solid particles makes the corrosion pits more concentrated.

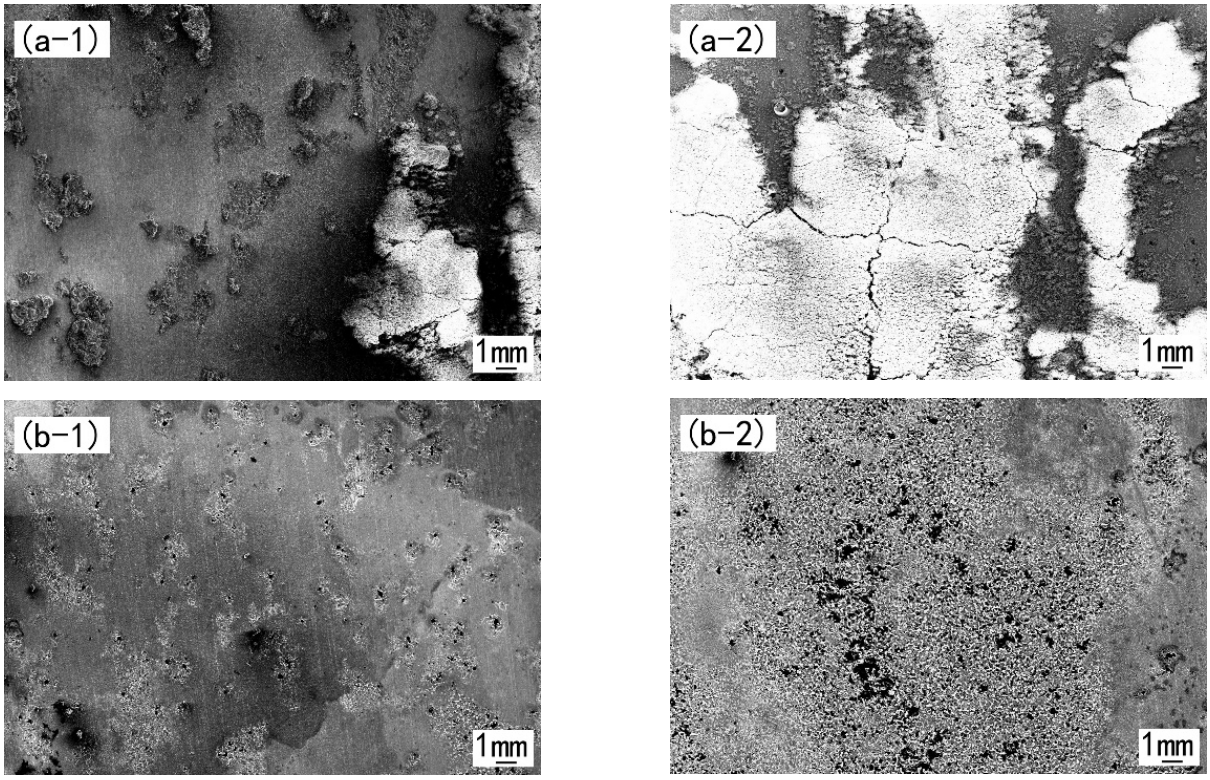

Figure 10. Surface topography of the pure corrosion test electrode: (**a**) before chemical cleaning, (**b**) after chemical cleaning.

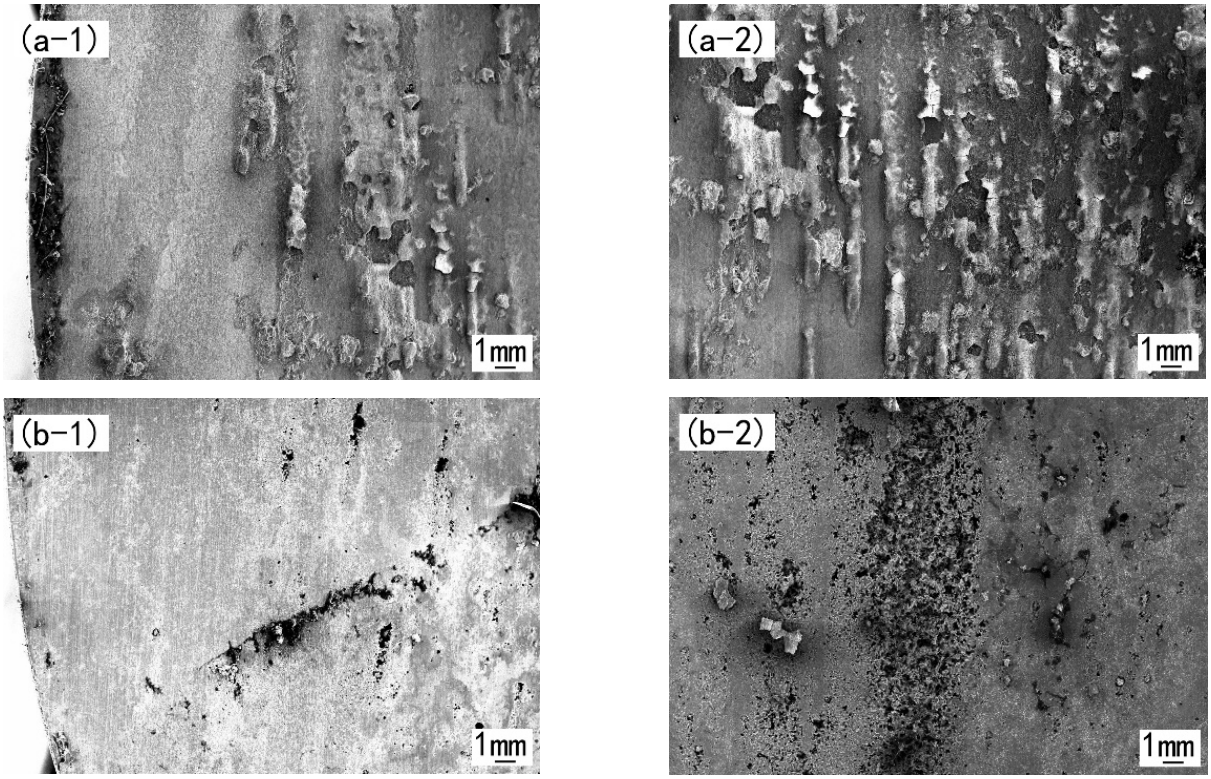

Figure 11. Surface topography of the erosion-corrosion test electrode: (**a**) before chemical cleaning, (**b**) after chemical cleaning.

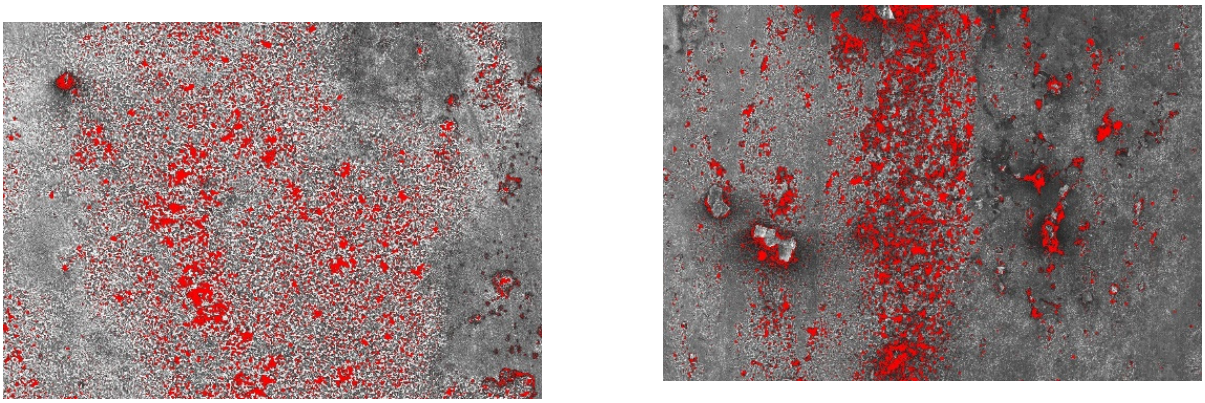

(**a**) (**b**)

Figure 12. Pit area to whole area ratio of (**a**) pure corrosion test electrode and (**b**) erosion corrosion test electrode.

Corrosion pits were observed both in the pure corrosion test and erosion-corrosion test, while the localized corrosion behavior was only observed in the EIS diagrams performed in the oil-water-sand system. Obviously, the addition of solid particles makes corrosion localization more apparent. As indicated in the research work of Xu et al., the synergy of sand and the anodic dissolution play an important role in the localized erosion-corrosion [36]. High concentration of Cl^- ions in the oilfield brine could undermine the passive film and hinder its formation on the steel surface, thus creating the anodic sites, which finally evolved into corrosion pits. This is true in both the oil-water solution and the oil-water-sand solution. Moreover, when the sand particles are added to the solution, they could destroy the passive film and corrosion product film on the local area of the substrate surface. Some initial anodic sites, which experience frequent sand impact, however, could maintain a high pitting propagation rate [36] when their nearby area was not, localized corrosion would then be intensified due to the big-cathode-to-small-anode effect [37].

4. Conclusions

A home-made testing pipe flow loop was designed and used to experimentally study the erosion-corrosion behavior of $20^{\#}$ steel in oil-water-sand multiphase flow under various flow conditions. With the increase of the flow velocity from 0.5 m/s to 2 m/s, the corrosion rate of $20^{\#}$ steel in the oil-water flow tended to go up on the whole, but did not follow a linear pattern. This is due to the mutual effect of the increased flow and the formation of the corrosion product film.

The addition of sand in the oil-water fluid could increase the corrosion rate after the sand concentration exceeded 1 wt%, but the contribution of sand erosion to corrosion was not always significant. Sand in the oil-water fluid could make the distribution of corrosion pits more concentrated in a local area and intensify the localized corrosion. After adding 2 wt% quartz sand, which had a size between 300 μm and 450 μm, into the oil-water fluid, pure corrosion and pure erosion accounted for 47.5% and 70.83% of the total erosion-corrosion, respectively, in the erosion-corrosion tests at the velocity of 2 m/s. The erosion-enhanced corrosion was 16.67% of the total erosion-corrosion, while the corrosion inhibiting the damage of erosion on $20^{\#}$ steel was 35.00% of the total erosion-corrosion.

Negative synergism appeared in the erosion-corrosion system. This is because the corrosion product film formed on the steel surface could decrease the friction between impacting solid particles and the bulk substrate material, and reduce the chances of the bare steel surface to be exposed to the sandy flow. However, due to the combined effect of Cl^- and the sand particles, localized failure of the corrosion product film happened on the steel surface. The steel surface that was not protected by the corrosion product film finally

evolved into localized corrosion sites and maintained a high propagation rate due to the big-cathode-to-small-anode effect.

Author Contributions: Conceptualization, Q.L.; methodology, B.L.; formal analysis, Q.L.; investigation, Q.L.; writing—original draft preparation, Q.L.; writing—review and editing, B.L. All authors have read and agreed to the published version of the manuscript.

Funding: This research was funded by the National Natural Science Foundation of China, grant number 40706031, and the Shandong Province Natural Science Foundation, grant number ZR2019BEE040.

Data Availability Statement: Data presented in this article are available at request from the corresponding author.

Acknowledgments: The authors thank Yan Li and Xiao Tang, both from the China University of Petroleum (East China), for providing electrochemical testing equipment in performing the experimental studies and for their technical support in finalizing this manuscript.

Conflicts of Interest: The authors declare no conflict of interest.

References

1. Islam, M.A.; Farhat, Z.N. The synergistic effect between erosion and corrosion of API pipeline in CO_2 and saline medium. *Tribol. Int.* **2013**, *68*, 26–34. [CrossRef]
2. Qiao, Q.; Cheng, G.; Li, Y.; Wu, W.; Hu, H.; Huang, H. Corrosion failure analyses of an elbow and an elbow-to-pipe weld in a natural gas gathering pipeline. *Eng. Fail. Anal.* **2017**, *82*, 599–616. [CrossRef]
3. Chen, Y.; Wu, H.; Chen, Y.; Li, P.; Wang, Q. Erosion-corrosion coupling analysis of shale gas production pipe. *Eng. Fail. Anal.* **2022**, *138*, 106308. [CrossRef]
4. Jones, M.; Llewellyn, R.J. Erosion-corrosion assessment of materials for use in the resources industry. *Wear* **2009**, *267*, 2003–2009. [CrossRef]
5. Tang, X.; Xu, L.Y.; Cheng, Y.F. Electrochemical corrosion behavior of X-65 steel in the simulated oil–sand slurry. II: Synergism of erosion and corrosion. *Corros. Sci.* **2008**, *50*, 1469–1474. [CrossRef]
6. Lu, B.T.; Luo, J.L.; Guo, H.X.; Mao, L.C. Erosion-enhanced corrosion of carbon steel at passive state. *Corros. Sci.* **2011**, *53*, 432–440. [CrossRef]
7. Jia, W.; Zhang, Y.; Li, C.; Luo, P.; Song, X.; Wang, Y.; Hu, X. Experimental and numerical simulation of erosion-corrosion of 90° steel elbow in shale gas pipeline. *J. Nat. Gas Sci. Eng.* **2021**, *89*, 103871. [CrossRef]
8. El-Sayed, M.H. Flow enhanced corrosion of water injection pipelines. *Eng. Fail. Anal.* **2015**, *50*, 1–6. [CrossRef]
9. Aminul Islam, M.; Farhat, Z.N. Mechanical and Electrochemical Synergism of API X42 Pipeline Steel During Erosion–Corrosion. *J. Bio-Tribo-Corros.* **2015**, *1*, 26. [CrossRef]
10. Demoz, A.; Dabros, T. Relationship between shear stress on the walls of a pipe and an impinging jet. *Corros. Sci.* **2008**, *50*, 3241–3246. [CrossRef]
11. Ilman, M.N.; Kusmono, K. Analysis of internal corrosion in subsea oil pipeline. Case Stud. *Eng. Fail. Anal.* **2014**, *2*, 1–8.
12. Jiang, X.; Xu, K.; Guan, X.; Qu, D.; Song, X.; Zhang, Q.; Yu, C.; Hua, J. A comparative study on the corrosion of gathering pipelines in two sections of a shale gas field. *Eng. Fail. Anal.* **2021**, *121*, 105179. [CrossRef]
13. Khan, R.; Ya, H.H.; Pao, W.; Majid, M.A.A.; Ahmed, T.; Ahmad, A.; Alam, M.A.; Azeem, M.; Iftikhar, H. Effect of Sand Fines Concentration on the Erosion-Corrosion Mechanism of Carbon Steel 90 degrees Elbow Pipe in Slug Flow. *Materials* **2020**, *13*, 4601. [CrossRef]
14. Thaker, J.; Banerjee, J. Influence of intermittent flow sub-patterns on erosion-corrosion in horizontal pipe. *J. Pet. Sci. Eng.* **2016**, *145*, 298–320. [CrossRef]
15. Nassef, A.; Keller, M.; Hassani, S.; Shirazi, S.; Roberts, K. A Review of Erosion-Corrosion Models for the Oil and Gas Industry Applications. In *Recent Developments in Analytical Techniques for Corrosion Research*; Springer: Tulsa, OK, USA, 2022; pp. 205–233.
16. Wongpanya, P.; Saramas, Y.; Chumkratoke, C.; Wannakomol, A. Erosion–corrosion behaviors of 1045 and J55 steels in crude oil. *J. Pet. Sci. Eng.* **2020**, *189*, 106965. [CrossRef]
17. Peng, W.; Cao, X.; Ji, J.; Jin, X.; Wang, Q. Erosion of Pipe Bend and Plugged Tee by Solid Particles in Oil-water-sand multiphase flow. *Corros. Prot.* **2016**, *37*, 131–136. (In Chinese)
18. Stack, M.M.; Abdulrahman, G.H. Mapping erosion–corrosion of carbon steel in oil–water solutions: Effects of velocity and applied potential. *Wear* **2012**, *274–275*, 401–413. [CrossRef]
19. Meng, Q.; Han, W.; Wang, X.; Li, S.; Wang, C. Corrosive Wear Property of Material of Oil Tubing in Sand-Oil-Water Liquid. *Oil Field Equip.* **2008**, *37*, 52–54. (In Chinese)
20. Li, Q.; Hu, H.; Cheng, Y.F. Corrosion of pipelines in CO_2 saturated oil-water emulsion flow studied by electrochemical measurements and computational fluid dynamics modeling. *J. Pet. Sci. Eng.* **2016**, *147*, 408–415. [CrossRef]
21. Xu, Y.; Liu, L.; Zhou, Q.; Wang, X.; Tan, M.Y.; Huang, Y. An Overview of Major Experimental Methods and Apparatus for Measuring and Investigating Erosion-Corrosion of Ferrous-Based Steels. *Metals* **2020**, *10*, 180. [CrossRef]

22. Liu, J.; Wang, J.; Hu, W. Erosion–corrosion behavior of X65 carbon steel in oilfield formation water. *Int. J. Electrochem. Sci.* **2019**, *14*, 262–278. [CrossRef]
23. Cai, G.; Zhu, S.; Li, J.; Feng, Z.; Lv, L. Influencing Factors of Internal Corrosion of 20# Oil Field Gathering and Transmission Pipeline. *Corros. Prot.* **2016**, *37*, 653–656. (In Chinese)
24. Liu, Y.; Jiang, H.; Xu, T.; Li, Y. CO_2 corrosion prediction on 20# steel under the influence of corrosion product film. *Petroleum* **2021**, *in press*.
25. Li, M.; Ma, Y.; Yang, W.; Cai, L.; Liang, C. Influencing Factors of Internal Corrosion of Oil Gathering and Transportation Pipelines Based on Statistical Data. *Pet. Tubul. Goods Instrum.* **2022**, *8*, 43–47. (In Chinese)
26. Cui, P. Research on main influencing factors of internal corrosion of 20# oil field gathering and transmission pipeline. *Pet. Tubul. Goods Instrum.* **2022**, *8*, 42–46. (In Chinese)
27. Liu, J.; BaKeDaShi, W.; Li, Z.; Xu, Y.; Ji, W.; Zhang, C.; Cui, G.; Zhang, R. Effect of flow velocity on erosion–corrosion of 90-degree horizontal elbow. *Wear* **2017**, *376–377*, 516–525. [CrossRef]
28. *ASTM G1-03*; Standard Practice for Preparing, Cleaning, and Evaluating Corrosion Test Specimens. ASTM International: West Conshohocken, PA, USA, 2011.
29. Collins, T. Particle Analysis. ImageJ Docs. 2022. Available online: https://imagej.net/imaging/particle-analysis (accessed on 19 November 2022).
30. Barker, R.; Burkle, D.; Charpentier, T.; Thompson, H.; Neville, A. A review of iron carbonate ($FeCO_3$) formation in the oil and gas industry. *Corros. Sci.* **2018**, *142*, 312–341. [CrossRef]
31. Aminul Islam, M.; Farhat, Z.N.; Ahmed, E.M.; Alfantazi, A.M. Erosion enhanced corrosion and corrosion enhanced erosion of API X-70 pipeline steel. *Wear* **2013**, *302*, 1592–1601. [CrossRef]
32. Leng, J.; Frank Cheng, Y.; Liao, K.; Huang, Y.; Zhou, F.; Zhao, S.; Liu, X.; Zou, Q. Synergistic effect of O_2-Cl^- on localized corrosion failure of L245N pipeline in CO_2-O_2-Cl^- − environment. *Eng. Fail. Anal.* **2022**, *138*, 106332. [CrossRef]
33. Luo, Y. In Field Electrochemical Detection and Erosion-Corrosion Investigation of Metallic Materials in Marine Environment. Ph.D. Thesis, Tianjing University, Tianjin, China, 2007. (In Chinese).
34. Harvey, T.J.; Wharton, J.A.; Wood, R.J.K. Development of synergy model for erosion–corrosion of carbon steel in a slurry pot. Tribol. *Mater. Surf. Interfaces* **2013**, *1*, 33–47. [CrossRef]
35. Wood, R.J.K. Erosion–corrosion interactions and their effect on marine and offshore materials. *Wear* **2006**, *261*, 1012–1023. [CrossRef]
36. Xu, Y.; Zhang, Q.; Gao, S.; Wang, X.; Huang, Y. Exploring the effects of sand impacts and anodic dissolution on localized erosion-corrosion in sand entraining electrolyte. *Wear* **2021**, *478–479*, 203907. [CrossRef]
37. Zhang, G.A.; Cheng, Y.F. Localized corrosion of carbon steel in a CO_2-saturated oilfield formation water. *Electrochim. Acta* **2011**, *56*, 1676–1685. [CrossRef]